Published in final edited form as:

J Magn Reson Imaging. 2020 April ; 51(4): 1212–1222. doi:10.1002/jmri.26916.

Myocardial Velocity, Intra-, and Interventricular Dyssynchrony Evaluated by Tissue Phase Mapping in Pediatric Heart Transplant Recipients

Haben Berhane, MA[1,*], **Alexander Ruh, PhD**[2], **Nazia Husain, MBBS, MPH**[3,4], **Joshua D. Robinson, MD**[2,3,4], **Cynthia K. Rigsby, MD**[1,2,4], **Michael Markl, PhD**[2,5]

[1]Department of Medical Imaging, Ann & Robert H. Lurie Children's Hospital of Chicago, Chicago, Illinois, USA

[2]Department of Radiology, Feinberg School of Medicine, Northwestern University, Chicago, Illinois, USA

[3]Department of Pediatrics, Division of Pediatric Cardiology, Ann & Robert H. Lurie Children's Hospital of Chicago, Chicago, Illinois, USA

[4]Department of Pediatrics, Feinberg School of Medicine, Northwestern University, Chicago, Illinois, USA

[5]Department of Biomedical Engineering, McCormick School of Engineering, Northwestern University, Chicago, Illinois, USA

Abstract

Background: Endomyocardial biopsy (EMB) is the standard method for detecting allograft rejection in pediatric heart transplants (Htx). As EMB is invasive and carries a risk of complications, there is a need for a noninvasive alternative for allograft monitoring.

Purpose: To quantify left and right ventricular (LV & RV) peak velocities, velocity twist, and intra-/interventricular dyssynchrony using tissue phase mapping (TPM) in pediatric Htx compared with controls, and to explore the relationship between global cardiac function parameters and the number of rejection episodes to these velocities and intra-/interventricular dyssynchrony.

Study Type: Prospective.

Subjects: Twenty Htx patients (age: 16.0 ± 3.1 years, 11 males) and 18 age- and sex-matched controls (age: 15.5 ± 4.3 years, nine males).

Field Strength/Sequence: 5T; 2D balanced cine steady-state free-precession (bSSFP), TPM (2D cine phase contrast with three-directional velocity encoding).

Assessment: LV and RV circumferential, radial, and long-axis velocity–time curves, global and segmental peak velocities were measured using TPM. Short-axis bSSFP images were used to measure global LV and RV function parameters.

[*]Address reprint requests to: H.B., Ann & Robert H. Lurie Children's Hospital of Chicago, 225 E Chicago Ave., Chicago, IL 60611. hberhane@luriechildrens.org.

Statistical Tests: A normality test (Lilliefors test) was performed on all data. For comparisons, a *t*-test was used for normally distributed data or a Wilcoxon rank-sum test otherwise. Correlations were determined by a Pearson correlation.

Results: Htx patients had significantly reduced LV ($P < 0.05–0.001$) and RV ($P < 0.05–0.001$) systolic and diastolic global and segmental long-axis velocities, reduced RV diastolic peak twist ($P < 0.01$), and presented with higher interventricular dyssynchrony for long-axis and circumferential motions ($P < 0.05–0.001$). LV diastolic long-axis dyssynchrony ($r = 0.48$, $P = 0.03$) and RV diastolic peak twist ($r = −0.64$, $P = 0.004$) significantly correlated with the total number of rejection episodes.

Data Conclusion: TPM detected differences in biventricular myocardial velocities in pediatric Htx patients compared with controls and indicated a relationship between Htx myocardial velocities and rejection history.

Level of Evidence: 2

Technical Efficacy Stage: 3

WHILE THE SURVIVAL RATE of pediatric heart transplant (Htx) recipients has improved, many patients remain at risk for allograft rejection, especially in the first year posttransplant.[1] Consequently, monitoring Htx graft status for acute allograft rejection is critically important to prevent graft dysfunction and mortality in the long term. Currently, endomyocardial biopsy (EMB) is the reference standard technique for rejection monitoring. However, EMB has been associated with patient discomfort, potential tricuspid valve damage, and other more serious complications.[2,3] Tricuspid regurgitation remains a significant complication in pediatric Htx patients, with a reported incidence of 84%, and has increasingly been linked to the frequency of biopsy.[3–5] Further, there are issues of sampling errors, poor sample quality, and a high interobserver variability in biopsy reporting, raising concerns of EMB accuracy.[6,7] As such, there is a need for a more consistent and noninvasive technique to monitor allograft health.

Magnetic resonance imaging (MRI) has emerged as a potential noninvasive tool for assessing left ventricular (LV) myocardial changes in adult and pediatric Htx recipients. T_2 mapping and strain analysis demonstrate high specificity and sensitivity in predicting transplant rejection, adverse fibrotic remodeling, and cardiomyopathy.[8–10] While right ventricular (RV) function is more likely to be impaired in children compared with LV function posttransplant,[11,12] few studies have utilized MRI to explore RV myocardial changes.[13,14] Importantly, RV dysfunction has been linked to severe transplant complications, accounting for over 10% of early deaths after cardiac transplantation.[15] RV dysfunction is also an indicator of early graft rejection and mortality in Htx patients and is associated with increased likelihood of allograft rejection complications.[15–17]

While myocardial deformation is now routinely measured by conventional echocardiography and is starting to be used for clinical decision-making, several MR tools have also emerged to detect changes in segmental and regional contractility, dyssynchrony, twist, and torsion. Initial studies have shown that these advanced functional parameters are significantly reduced in adult and pediatric Htx recipients compared with controls, and that they may

predict development of rejection even in the presence of preserved ejection fraction (EF).[9,11,18–24] These techniques explore segmental myocardial abnormalities that may be occurring in Htx patients that cannot detected by standard measures of function.

In this study we explore tissue phase mapping (TPM) as a promising noninvasive MRI technique to explore cardiac function impairment in Htx recipients. TPM is a 2D phase contrast cine MRI technique that allows for assessment of myocardial contractility and function through the quantification of regional (segmental) velocities.[25] Prior studies have demonstrated that TPM can detect LV functional changes in many common cardiac conditions in adults, including systemic and pulmonary hypertension, dilated cardiomyopathy, and heart transplantation.[25–28] Recent advancements in TPM have enabled a faster, clinically feasible breath-hold scan acquisition and have demonstrated its utility in exploring both LV and RV myocardial velocities in healthy adults and adults with hypertension.[29]

Hence, the goal of this study was to examine LV and RV peak velocities, interventricular dyssynchrony, and velocity twists to detect significant differences and myocardial functional abnormalities in pediatric Htx patients compared with controls. Additionally, we explored correlations between the global peak TPM velocities, global function parameters, time after transplant, and the number of rejection episodes.

Patients and Methods

Study Cohort

Patient and control demographics are summarized in Table 1. The study cohort was comprised of 20 pediatric Htx patients (age: 16.0 ± 3.1 years, 11 males) and 18 age-matched pediatric healthy controls (age: 15.5 ± 4.3 years, nine males) without known cardiac disease. Htx patients and controls were age- and sex-matched ($P = 0.66$ and 0.77, respectively). All subjects underwent a physician-ordered standard-of-care MR including TPM. This HIPAA-compliant study was approved by the local Institutional Review Board (IRB). Informed consent was acquired from each patient and/or his/her parents for the TPM sequence per IRB requirements. Controls were excluded if there were any known clinical abnormalities or if abnormalities were found on the MR study.

Transplant Surveillance

All Htx patients received annual EMB following transplant. The total number of rejection episodes was determined from the number of incidences of acute allograft rejection in the EMB reports across the patient's history. Rejection grade was recorded as mild (1R), moderate (2R), or severe (3R) grades and noted for the presence of antibody-mediated rejection (AMR) as defined by the International Society for Heart & Lung Transplantation (ISHLT) grading scheme.[30] Each reported incidence of rejection was counted the same, regardless of biopsy grading. The total number of rejection episodes at each rejection grade for each patient in the Htx cohort is provided in the Appendix, Table A1.

Cardiac MRI

MR was performed at 1.5T (Aera, Siemens, Erlangen, Germany) and included retrospectively ECG-gated 2D cine balanced steady-state free-precession (bSSFP) imaging and TPM for the assessment of global and regional biventricular function. 2D cine bSSFP images of the ventricles were obtained in short-axis (stack) and long-axis (2 chamber, 4 chamber, 3 chamber) orientations. Imaging parameters were as follows: repetition time / echo time (TR/TE) = 2.8–3.1 / 1.23–1.34 msec; flip angle = 90°, slice thickness = 5–7 mm, in-plane resolution = (0.94–1.31 mm),^{2} parallel imaging (GRAPPA technique) with acceleration factor R = 2.

TPM was acquired during breath-holding and using a prospectively ECG gated, three-directional velocity-encoded, and black-blood prepared gradient echo sequence as previously described.[31] TPM images were obtained in the short-axis orientation at the ventricular base, mid-ventricle, and apex. Imaging parameters were: temporal resolution = 20.8–24.8 msec, TE/TR = 3.4–3.5/5.2–6.2 msec, in-plane resolution = (1.5–2.5 mm),^{2} slice thickness = 5–8 mm, velocity sensitivity (venc) = 25 cm/s. Spatiotemporal imaging acceleration (k-t parallel imaging PEAK GRAPPA) with a net acceleration factor of R_{net} = 3.5–3.9 was employed, which permitted data acquisition during breath-holding.[32]

Data Analysis

LV and RV volumes and ejection fractions were determined from short-axis cine SSFP images using commercial software (Medis Qmass, Leiden, Netherlands). The epi- and endocardium were manually contoured on short-axis cine SSFP images to generate the global function parameters of left and right ventricular end-systolic volumes (LVESV, RVESV), left and right ventricular end-diastolic volumes (LVEDV, RVEDV), and left and right ventricular stroke volumes (LVSV, RVSV). These parameters were indexed to body surface area.

TPM postprocessing was performed using in-house-developed software in MatLab (MathWorks, Natick, MA). The workflow involved manual contouring (Fig. 1a) of the LV and RV epi- and endocardium across all three slices (base, mid, apex) and time frames for all controls and patients as described previously.[31] After correcting for eddy currents, the acquired time-resolved velocity data was transformed from Cartesian coordinates (v_y, v_x, v_z) to cylindrical coordinates in radial (v_r,), circumferential (v_φ), and long-axis (v_z) motion components adapted to the motion components of the heart (Fig. 1b). Positive values represent contraction (v_r), clockwise rotation (v_φ), or shortening (v_z). From the segmented LV and RV myocardium, slice-average velocity-time curves are generated for each of the motion components (Fig. 1c). An American Heart Association (AHA) 16 segment LV model[33] with a 10 segment RV (Fig. 1d) expansion was used for segmental velocity analyses. For each LV and RV segment, systolic and diastolic peak velocities were determined. Global LV and RV peak velocities were calculated as the average of the peak segmental velocities for each ventricle. For circumferential (v_φ) motion, the peak systolic and diastolic twist velocities were quantified as the difference between slice-averaged circumferential velocities from base and apex across all cardiac time frames. Intraventricular dyssynchrony was calculated for v_r and v_z as the standard deviation of the time-to-peak for

systole and diastole across the segments of the LV (16 segments) and RV (10 segments). Interventricular dyssynchrony was determined by the cross-correlation coefficient (cc) between the slice-averaged LV and RV velocity time courses. A single cc was determined for each motion component across all three slices and measures the degree of dyssynchrony as a value between 0 and 1 (with 1 indicating complete synchrony between the LV and RV, and 0 denoting complete dyssynchrony).

Statistics

All data are reported as means ± standard deviations. To determine any significant differences, first a Lilliefors test was used to determine normality, and then an unpaired *t*-test for normally distributed data or a Wilcoxon rank-sum test for nonnormally distributed data were performed between the Htx cohort and the healthy controls for each segment in the 16 + 10 LV-RV model as well as for the global peak velocities, inter-, and intraventricular dyssynchrony across the LV and RV. Additionally, Pearson's correlation coefficients (r) were calculated for Htx patients to determine the relationship between global peak TPM velocities, inter-, and intraventricular dyssynchrony to the global function parameters, time after transplant, and the number of rejection episodes. Significance was determined by $P < 0.05$.

Results

Study Cohort and Global Cardiac Function Parameters

MR was performed on average 5.9 ± 5.4 years posttransplant, with a range of 0.9–19.5 years. Global right and left ventricular volumetric and ejection fraction values for the cohorts were similar between the Htx patients and controls (Table 1). The indexed left ventricular end-diastolic volume (LVEDVI) was found to be significantly different between the Htx patients and controls.

During TPM data analysis, two Htx patients could not have the RV contoured in the apical slices due to poor resolution between the myocardium and blood pool on these images. Additionally, in two patients the basal slices were too close to the mitral valve, resulting in the RV outflow tract becoming included in the anterior RV wall. In those cases, the anterior basal RV segment was excluded from the analysis.

Biventricular Velocities: Transplant Patients vs. Controls

The global systolic and diastolic RV and LV velocities are summarized in Table 2. Long-axis velocities were significantly reduced in Htx patients during systole and diastole for both the LV (systole: $P = 0.003$, diastole: $P < 0.001$) and RV (systole: $P < 0.001$, diastole: $P < 0.001$) compared with controls. Further, peak twist velocities in the RV were significantly reduced for Htx patients during systole ($P = 0.002$) and diastole ($P = 0.007$).

An example of the contrasting myocardial velocity and velocity-time curves for a Htx patients and a control is provided in Fig. 2. Segmental differences are depicted in Figs. 3 and 4. For long-axis motion (Fig. 3), 9/16 segments during systole (2/16: $P < 0.05$, 7/16: $P < 0.01$) and 15/16 segments during diastole (3/16: $P < 0.05$, 12/16: $P < 0.01$) were found to

have significantly reduced long-axis velocities in the LV for Htx patients compared with controls. In the RV, 7/10 segments during systole (2/10: $P < 0.05$, 5/10: $P < 0.01$) and 10/10 segments during diastole (2/10: $P < 0.05$, 8/10: $P < 0.01$) had significantly reduced long-axis velocities in Htx patients. For radial motion (Fig. 4), 3/16 segments during systole (3/16: $P < 0.05$) and 4/16 for diastole (2/16: $P < 0.05$, 2/16: $P < 0.01$) had significantly lower velocities in Htx patients when compared with controls in the LV, while 2/10 segments during systole (1/10: $P < 0.05$, 1/10: $P < 0.01$) and 3/10 during diastole (3/10: $P < 0.05$) were found to be significantly reduced in the RV. For intraventricular dyssynchrony, Htx had higher diastolic RV dyssynchrony for v_z motion (Htx: 77.9 ± 29.9 msec, controls: 42.1 ± 15.8, $P < 0.01$). Additionally, Htx patients were found to have increased interventricular dyssynchrony in the circumferential (cc = 0.53 ± 0.23 vs. 0.73 ± 0.16, $P = 0.004$) and long-axis directions (cc = 0.43 ± 0.20 vs. 0.64 ± 0.15, $P = 0.001$) compared with controls.

Biventricular Velocities: Relationship With Heart Characteristics

Correlation results between Htx global velocities and global function parameters are summarized in Table 3. For LV velocities, systolic peak v_r and peak twist were positively correlated with the LV (LVSVI; v_r: $r = 0.71$, $P < 0.01$; twist: $r = 0.65$, $P < 0.01$) and RV (RVSVI; v_r: $r = 0.65$, $P < 0.01$; twist: $r = 0.56$, $P < 0.05$) indexed stroke volume and LV (LVEF; v_r: $r = 0.47$, $P < 0.05$; twist: $r = 0.69$, $P < 0.01$) and RV (RVEF; v_r: $r = 0.52$, $P < 0.05$, twist: $r = 0.48$, $P < 0.05$) ejection fractions. Additionally, LV diastolic peak v_r positively correlated with the LV indexed end-diastolic volume (LVEDVI; $r = 0.48$, $P < 0.05$) and RVSVI ($r = 0.53$, $P < 0.05$). For RV velocities, systolic peak v_r and peak twist were positively correlated with the LVSVI (twist: $r = 0.59$, $P < 0.01$), RVSVI (twist: $r = 0.62$, $P < 0.01$), and RVEF (v_r: $r = 0.58$, $P < 0.05$; twist: $r = 0.53$, $P < 0.05$). For the LV dyssynchrony, LV systolic v_z dyssynchrony was positively correlated with the LVEF ($r = 0.48$, $P < 0.05$) and RVEF ($r = 0.54$, $P < 0.05$). For RV dyssynchrony, RV systolic v_z dyssynchrony had a similar positive correlation with the LVEF ($r = 0.46$, $P < 0.05$) and RVEF ($r = 0.59$, $P < 0.01$), and an inverse correlation with the LVSVI ($r = -0.60$, $P < 0.01$) and RVSVI ($r = -0.64$, $P < 0.01$). There were no significant correlation with interventricular dyssynchrony.

As shown in Fig. 5, two significant correlations were found with the total number of rejection episodes for the Htx patients, a positive correlation with the diastolic LV vz dyssynchrony ($r = 0.47$, $P < 0.05$), and a negative correlation with the diastolic RV peak twist ($r = -0.65$, $P < 0.01$). No other global or segmental velocity components were found to correlate with the number of rejection episodes in our Htx cohort. There were no significant correlations found with time after transplantation.

Discussion

This study demonstrates the utility of TPM in exploring left and right myocardial velocities in pediatric Htx recipients. Globally and segmentally, Htx patients demonstrated significantly reduced systolic and diastolic left and right ventricular velocities compared with healthy controls. The most significant differences were found for the long-axis velocities, with Htx patients having impaired ventricular shortening and elongation.

Additionally, a moderate negative correlation was found between the right ventricular diastolic peak twist with the total number of rejection episodes of the Htx patients. The right ventricle (both globally and segmentally) had the most significant differences in long-axis velocities and peak twist in Htx patients compared with controls. Also, the Htx patients displayed greater interventricular dyssynchrony compared with controls for circumferential and long-axis motion.

Our findings are in agreement with previous studies exploring adult and pediatric Htx myocardial function with echocardiographic strain analysis and tissue Doppler imaging.[11,18–22] Saleh et al found a significant reduction in mean global longitudinal strain and strain rate in 80 adult Htx patients compared with 80 healthy controls using echocardiographic myocardial strain.[19] Likewise, Chinali et al showed similar results with global LV and RV longitudinal strain being significantly reduced in children and young adults following Htx compared with healthy controls.[21] Additionally, several adult and pediatric studies have shown a significant reduction in myocardial velocities and deformation by echocardiography to be associated with or predictive of graft rejection and failure.[34–36]

Comparing TPM in Htx patients to controls has yielded mixed results.[25,37,38] Markl et al found reduced LV diastolic long-axis and radial velocities[25] while Dolan et al found reduced LV systolic long-axis velocities and increased diastolic LV radial velocities in Htx patients.[38] We found both reduced systolic and diastolic LV and RV long-axis velocities in the pediatric Htx recipients. There were minimal differences in radial velocities in our pediatric cohort. The disparity may be a result of a more dramatic and adaptive cardiac remodeling in children compared with adults.[39]

RV failure has been linked in pediatric Htx to clinical variables like donor age and elevated pretransplant pulmonary vascular resistance index.[12] While the importance of RV dysfunction for graft failure has been established, with early RV dysfunction directly linked to early posttransplant morbidity and mortality,[16] few studies have assessed RV mechanics in evaluating graft health. Echocardiographic studies have found that altered or impaired RV parameters are more sensitive in detecting graft failure than LV parameters[34,35]; however, accurate Doppler-based velocity quantification can be difficult due to irregular RV geometry.[21,36] The strongest differentiator in our cohort also was segmental and global RV motion components, which showed significant impairment in the Htx recipients compared with controls. Additionally, we found that our Htx cohort had a greater frequency of rejection episodes compared with other institutions,[40] which allowed us to explore the impact on TPM functions across a wide range of rejection episodes. While our study is not large enough to explore the possibility that altered RV parameters can indicate graft failure, there was a moderate correlation between right ventricular diastolic circumferential motion and the number of rejection episodes in our cohort, suggesting that repeated rejection episodes result in abnormal RV remodeling in pediatric Htx patients. Further study of RV function by TPM in a larger post-Htx population is warranted.

Limitations of our study include the small cohort size, with only 20 Htx patients and 18 age-matched controls. Our Htx cohort had a wide range of posttransplant time (mean posttransplant time 5.9 ± 5.4 years; range 0.9–19.5 years), limiting temporal comparison of

myocardial velocities. There were also only three Htx patients with moderate or severe allograft rejection (≥2R). As a result, the impact of severity of allograft rejection on myocardial velocities could not be determined. Additionally, we do not have echocardiogram strain data on any of the Htx patients of our cohort, and, as a result, are unable to compare the TPM velocity data to echocardiogram strain data.

In conclusion, significant differences were found between Htx patients and controls for global and segmental long-axis and twist RV and LV velocities and Htx patients displayed greater interventricular dyssynchrony in the long-axis and circumferential motion compared with controls. Further, LV diastolic long-axis dyssynchrony was found to have a moderately positive correlation and RV diastolic peak twist with a moderately negative correlation with the number of rejection episodes in our Htx cohort. Further work in a larger cohort is needed to determine the utility of TPM as a noninvasive alternative to EMB for pediatric Htx graft monitoring.

Acknowledgments

Contract grant sponsor: National Institute of Heart, Lung and Blood Disorders (NHLBI); Contract grant number: R01 HL 117888.

APPENDIX 1:

TABLE A1.

Total number of rejection episodes for each Htx patient. The rejection grades and incidence were based on biopsy reporting. The total number of rejections was based on counting each reported rejection episode (1R, 2R, 3R, AMR) throughout the patient's history. Antibody-mediated rejection (AMR) was counted the same as a 1R.

Patients	Grade 1R	Grade 2R	Grade 3R	AMR	Total number of rejections
1	3				3
2	3				3
3	7			1	8
4	5				5
5	2			1	3
6	0				0
7	4				4
8	4				4
9	4	1			5
10	7				7
11	6				6
12	1				1
13	6	1	1	1	9
14	5			1	6
15	5				5
16	2				2

Patients	Grade 1R	Grade 2R	Grade 3R	AMR	Total number of rejections
17	7		2		9
18	5				5
19	2				2
20	6				6

References

1. Gradek WQ, D'Amico C, Smith AL, Vega D, Book WM. Routine surveillance endomyocardial biopsy continues to detect significant rejection late after heart transplantation. J Heart Lung Transplant 2001;20: 497–502. [PubMed: 11343975]
2. Saraiva F, Matos V, Goncalves L, Antunes M, Providencia LA. Complications of endomyocardial biopsy in heart transplant patients: A retrospective study of 2117 consecutive procedures. Transplant Proc 2011; 43:1908–1912. [PubMed: 21693299]
3. Huddleston CB, Rosenbloom M, Goldstein JA, Pasque MK. Biopsy-induced tricuspid regurgitation after cardiac transplantation. Ann Thorac Surg 1994;57:832–836; discussion 6–7. [PubMed: 8166527]
4. Kwon MH, Shemin RJ. Tricuspid valve regurgitation after heart transplantation. Ann Cardiothorac Surg 2017;6:270–274. [PubMed: 28706871]
5. Lo CY, Chang HH, Hsu CP, Lai ST, Shih CC. Endomyocardial biopsy-related tricuspid regurgitation after orthotopic heart transplantation: Single-center experience. J Chin Med Assoc 2007;70:185–192. [PubMed: 17524995]
6. Shah KB, Flattery MP, Smallfield MC, et al. Surveillance endomyocardial biopsy in the modern era produces low diagnostic yield for cardiac allograft rejection. Transplantation 2015;99:e75–80. [PubMed: 25706277]
7. Butler CR, Savu A, Bakal JA, et al. Correlation of cardiovascular magnetic resonance imaging findings and endomyocardial biopsy results in patients undergoing screening for heart transplant rejection. J Heart Lung Transplant 2015;34:643–650. [PubMed: 25934478]
8. Marie PY, Angioi M, Carteaux JP, et al. Detection and prediction of acute heart transplant rejection with the myocardial T2 determination provided by a black-blood magnetic resonance imaging sequence. J Am Coll Cardiol 2001;37:825–831. [PubMed: 11693758]
9. Grotenhuis HB, Nyns ECA, Kantor PF, et al. Abnormal myocardial contractility after pediatric heart transplantation by cardiac MRI. Pediatr Cardiol 2017;38:1198–1205. [PubMed: 28555404]
10. Vermes E, Pantaleon C, Auvet A, et al. Cardiovascular magnetic resonance in heart transplant patients: Diagnostic value of quantitative tissue markers: T2 mapping and extracellular volume fraction, for acute rejection diagnosis. J Cardiovasc Magn Reson 2018;20:59. [PubMed: 30153847]
11. Pauliks LB, Pietra BA, DeGroff CG, et al. Non-invasive detection of acute allograft rejection in children by tissue Doppler imaging: Myocardial velocities and myocardial acceleration during isovolumic contraction. J Heart Lung Transplant 2005;24(7 Suppl):S239–248. [PubMed: 15993780]
12. Lunze FI, Colan SD, Gauvreau K, et al. Cardiac allograft function during the first year after transplantation in rejection-free children and young adults. Circ Cardiovasc Imaging 2012;5:756–764. [PubMed: 23001896]
13. Brittain EL, Hemnes AR, Keebler M, Lawson M, Byrd BF 3rd, Disalvo T. Right ventricular plasticity and functional imaging. Pulm Circ 2012;2: 309–326. [PubMed: 23130100]
14. Amsallem M, Kuznetsova T, Hanneman K, Denault A, Haddad F. Right heart imaging in patients with heart failure: A tale of two ventricles. Curr Opin Cardiol 2016;31:469–482. [PubMed: 27467173]
15. Stobierska-Dzierzek B, Awad H, Michler RE. The evolving management of acute right-sided heart failure in cardiac transplant recipients. J Am Coll Cardiol 2001;38:923–931. [PubMed: 11583860]

16. Clemmensen TS, Eiskjaer H, Logstrup BB, Andersen MJ, Mellemkjaer S, Poulsen SH. Echocardiographic assessment of right heart function in heart transplant recipients and the relation to exercise hemodynamics. Transpl Int 2016;29:909–920. [PubMed: 27159372]
17. Yerebakan C, Buz S, Huebler M, Weng Y, Lehmkuhl H, Hetzer R. Right ventricular failure following heart transplantation—recovery after extended mechanical support. J Card Surg 2008;23:578–580. [PubMed: 18928498]
18. Godown J, Dodd DA, Stanley M, et al. Changes in left ventricular strain parameters following pediatric heart transplantation. Pediatr Transplant 2018;22:e13166. [PubMed: 29575396]
19. Saleh HK, Villarraga HR, Kane GC, et al. Normal left ventricular mechanical function and synchrony values by speckle-tracking echocardiography in the transplanted heart with normal ejection fraction. J Heart Lung Transplant 2011;30:652–658. [PubMed: 21193327]
20. Kailin JA, Miyamoto SD, Younoszai AK, Landeck BF. Longitudinal myocardial deformation is selectively decreased after pediatric cardiac transplantation: A comparison of children 1 year after transplantation with normal subjects using velocity vector imaging. Pediatr Cardiol 2012;33:749–756. [PubMed: 22367550]
21. Chinali M, Esposito C, Grutter G, et al. Cardiac dysfunction in children and young adults with heart transplantation: A comprehensive echocardiography study. J Heart Lung Transplant 2017;36:559–566. [PubMed: 28041955]
22. Syeda B, Hofer P, Pichler P, et al. Two-dimensional speckle-tracking strain echocardiography in long-term heart transplant patients: A study comparing deformation parameters and ejection fraction derived from echocardiography and multislice computed tomography. Eur J Echocardiogr 2011;12:490–96. [PubMed: 21636605]
23. Colquitt JL, Jeewa A, Morris SA, et al. Diminished global longitudinal strain predicts late allograft failure in pediatric heart transplant recipients. JACC Cardiovasc Imaging 2017;10:1529–1531. [PubMed: 28330655]
24. Tseng AS, Gorsi US, Barros-Gomes S, et al. Use of speckle-tracking echocardiography-derived strain and systolic strain rate measurements to predict rejection in transplant hearts with preserved ejection fraction. BMC Cardiovasc Disord 2018;18:241. [PubMed: 30579333]
25. Markl M, Rustogi R, Galizia M, et al. Myocardial T2-mapping and velocity mapping: Changes in regional left ventricular structure and function after heart transplantation. Magn Reson Med 2013;70:517–526. [PubMed: 23008092]
26. Foell D, Jung BA, Germann E, et al. Segmental myocardial velocities in dilated cardiomyopathy with and without left bundle branch block. J Magn Reson Imaging 2013;37:119–126. [PubMed: 22987362]
27. Foell D, Jung B, Germann E, Staehle F, Bode C, Markl M. Hypertensive heart disease: MR tissue phase mapping reveals altered left ventricular rotation and regional myocardial long-axis velocities. Eur Radiol 2013; 23:339–347. [PubMed: 22886534]
28. Knight DS, Steeden JA, Moledina S, Jones A, Coghlan JG, Muthurangu V. Left ventricular diastolic dysfunction in pulmonary hypertension predicts functional capacity and clinical worsening: A tissue phase mapping study. J Cardiovasc Magn Reson 2015;17:116. [PubMed: 26715551]
29. Kowalik GT, Muthurangu V, Khushnood A, Steeden JA. Rapid breath-hold assessment of myocardial velocities using spiral UNFOLD-ed SENSE tissue phase mapping. J Magn Reson Imaging 2016;44: 1003–1009. [PubMed: 26929195]
30. Lund LH, Edwards LB, Dipchand AI, et al. The Registry of the International Society for Heart and Lung Transplantation: Thirty-third Adult Heart Transplantation Report-2016; Focus Theme: Primary Diagnostic Indications for Transplant. J Heart Lung Transplant 2016;35: 1158–1169. [PubMed: 27772668]
31. Ruh A, Sarnari R, Berhane H, et al. Impact of age and cardiac disease on regional left and right ventricular myocardial motion in healthy controls and patients with repaired tetralogy of Fallot. Int J Cardiovasc Imaging 2019 [Epub ahead of print].
32. Jung B, Honal M, Ullmann P, Hennig J, Markl M. Highly k-t-space-accelerated phase-contrast MRI. Magn Reson Med 2008;60: 1169–1177. [PubMed: 18958854]

33. Cerqueira MD, Weissman NJ, Dilsizian V, et al. Standardized myocardial segmentation and nomenclature for tomographic imaging of the heart. A statement for healthcare professionals from the Cardiac Imaging Committee of the Council on Clinical Cardiology of the American Heart Association. Circulation 2002;105:539–542. [PubMed: 11815441]

34. Friedberg MK. Echocardiographic detection of heart transplant graft dysfunction: A new twist on an old theme. Circ Cardiovasc Imaging 2016;9(9).

35. Fyfe DA, Ketchum D, Lewis R, et al. Tissue Doppler imaging detects severely abnormal myocardial velocities that identify children with preterminal cardiac graft failure after heart transplantation. J Heart Lung Transplant 2006;25:510–517. [PubMed: 16678028]

36. Fyfe DA, Mahle WT, Kanter KR, Wu G, Vincent RN, Ketchum DL. Reduction of tricuspid annular Doppler tissue velocities in pediatric heart transplant patients. J Heart Lung Transplant 2003;22:553–559. [PubMed: 12742418]

37. Foll D, Markl M, Menza M, et al. Cold ischaemic time and time after transplantation alter segmental myocardial velocities after heart transplantation. Eur J Cardiothorac Surg 2014;45:502–508. [PubMed: 24026855]

38. Dolan RS, Rahsepar AA, Blaisdell J, et al. Cardiac structure-function MRI in patients after heart transplantation. J Magn Reson Imaging 2019;49:678–687. [PubMed: 30142237]

39. Delmo Walter EM, Huebler M, Stamm C, et al. Adaptive growth and remodeling of transplanted hearts in children. Eur J Cardiothorac Surg 2011;40:1374–1382; discussion 82–83. [PubMed: 21903412]

40. Huebler M, Schubert S, Lehmkuhl HB, et al. Pediatric heart transplantation: 23-year single-center experience. Eur J Cardiothorac Surg 2011; 39:e83–89. [PubMed: 21354807]

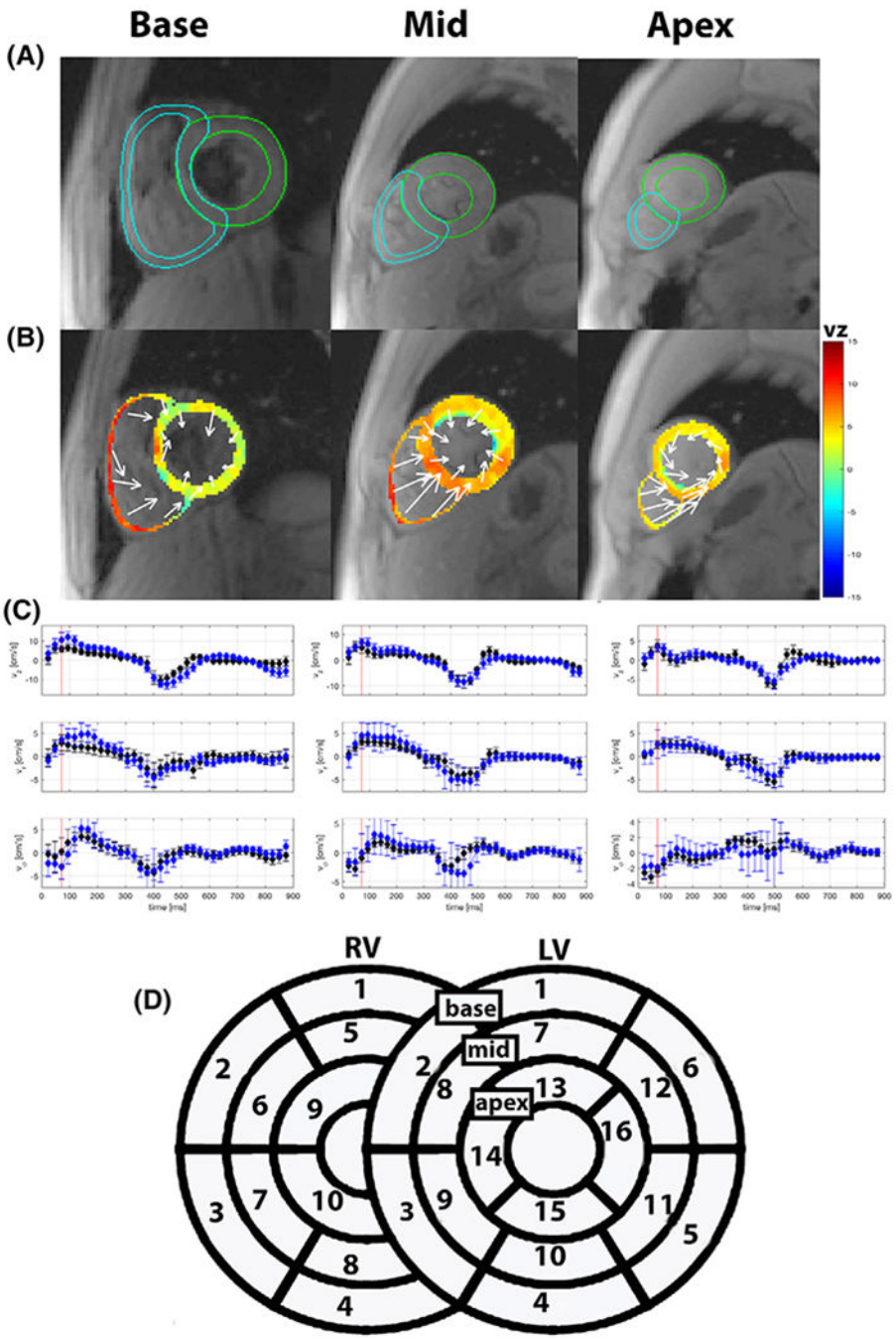

FIGURE 1:

TPM data analysis. Epicardial and endocardial RV and LV contours were manually drawn across all three slices **(a)**. From these contours, myocardial velocities were extracted. The velocities are displayed with color-coded long-axis velocities (through-plane) and in-plane velocity vectors **(b)**. LV and RV velocities were converted from Cartesian coordinates to long-axis, radial and circumferential directions. Slice averaged velocity–time curves **(c)** for each velocity component were obtained from the segmented LV and RV (black: left

ventricle, blue: right ventricle). Peak radial and long-axis velocities were extracted from the velocity–time curves for each segment in an extended 16 + 10 AHA model **(d)**

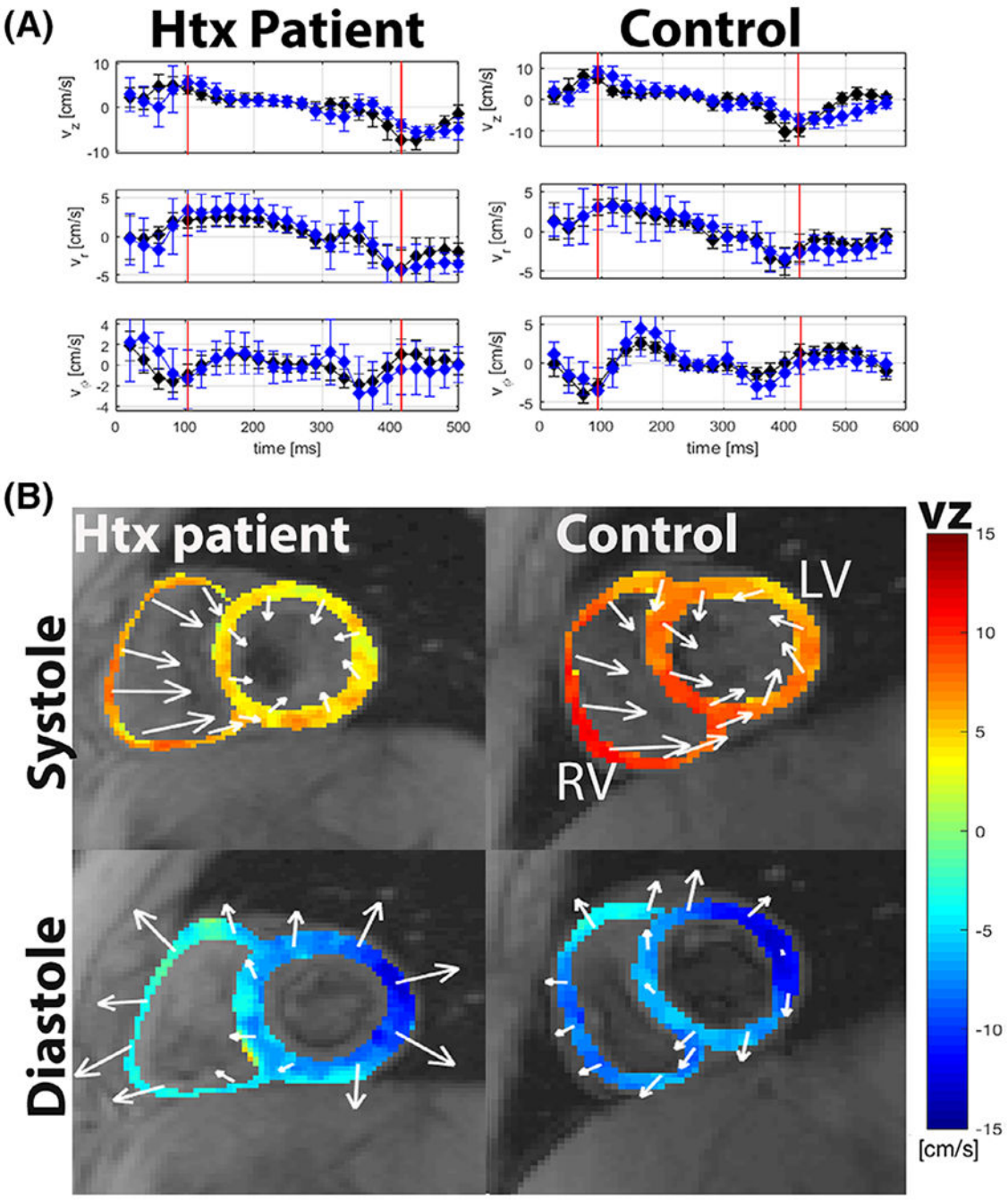

FIGURE 2:

Myocardial velocities in the basal slice compared between a Htx patient (age = 14 years) and a control subject (age = 15 years). **a:** Velocity–time curves for each velocity component (from top to bottom: long-axis velocities (v_z), radial velocities (v_r), and circumferential velocities (v_φ) are displayed for the Htx patient (left) and control subject (right). **b:** Examples of color-coded myocardial long-axis (v_z) velocity differences between Htx patient and control at the indicated timepoints (red lines in a) in the velocity–time curves. The color bar on the right indicates the long-axis velocity values, while the arrows represent the

regional in-plane velocity vectors. The Htx patient had lower long-axis velocities at both systole and diastole compared with the control.

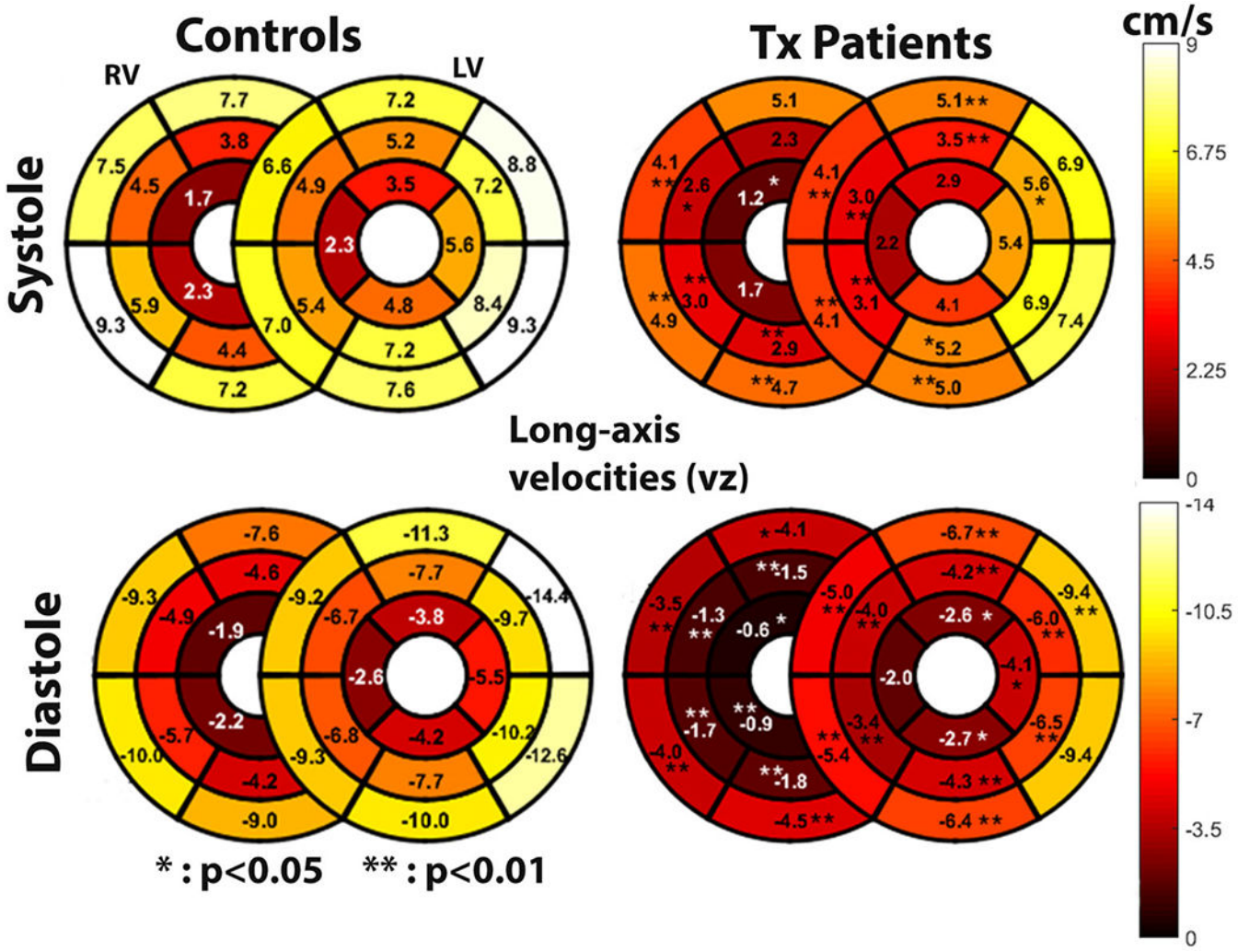

FIGURE 3:

Comparison of segmental velocities between Htx patients (right) and controls (left) for long-axis systolic (upper row) and diastolic (lower row) velocities. The bulls-eye plots are color-coded to indicate lower (darker color) to higher velocities (lighter colors) across the 16 + 10 AHA LV + RV segments. For the LV, 9/16 segments during systole and 15/16 segments during diastole were found to have significantly reduced velocities in Htx patients. For the RV, velocities in 7/10 segments during systole and 10/10 during diastole were significantly reduced. Significance is denoted by $*P < 0.05$ and $**P < 0.01$.

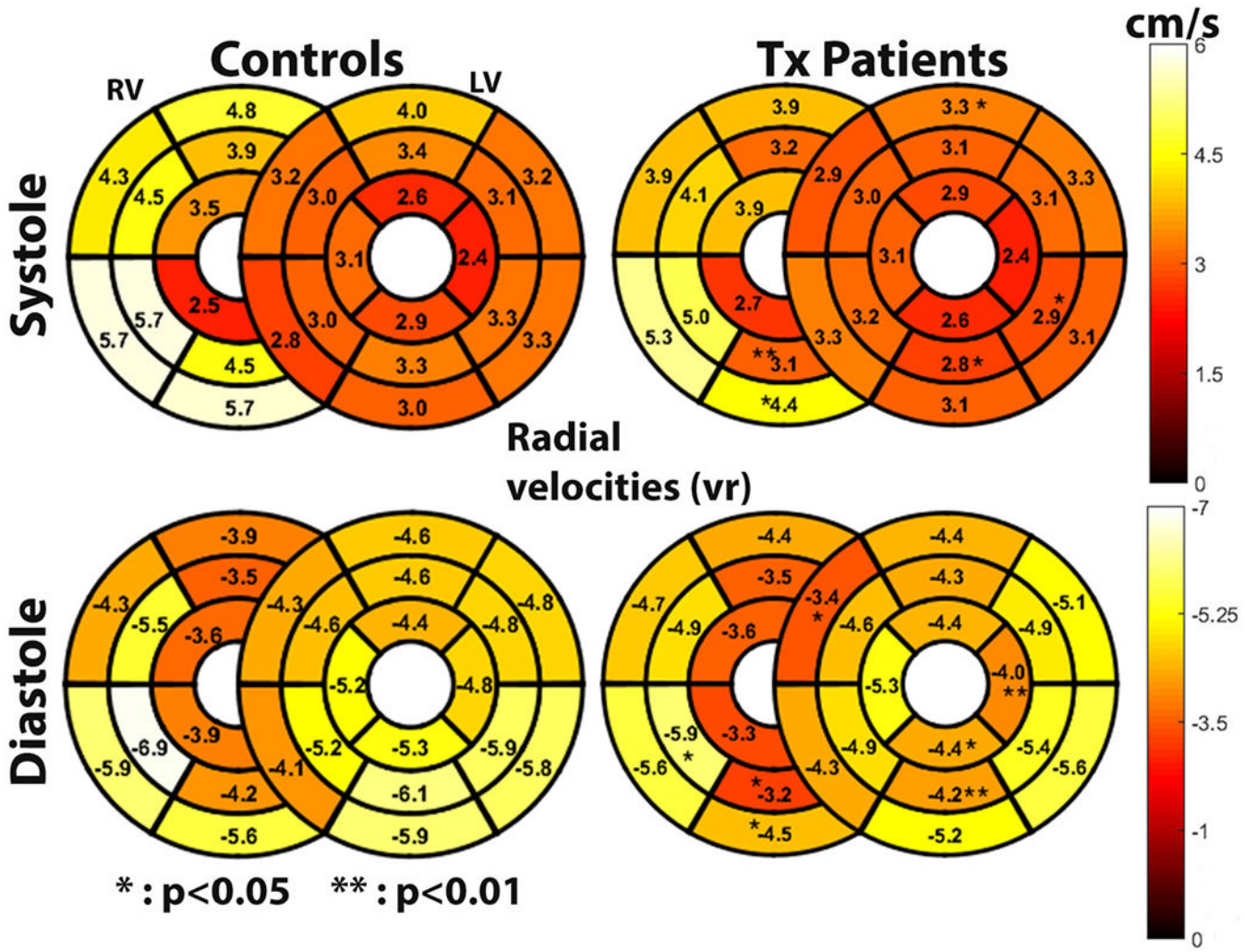

FIGURE 4:

Comparison of segmental velocities between Htx patients (right) and controls (left) for radial systolic (upper row) and diastolic (lower row) velocities. The color-coded bulls-eye plots visualize the difference in velocity across the 16 + 10 AHA LV + RV segments. For the LV, 3/16 segments during systole and 4/16 during diastole were found to have significantly reduced velocities in Htx patients, while for the RV, velocities in 2/10 segments during systole and 3/10 during diastole were significantly reduced. Significance is denoted by $*P < 0.05$ and $**P < 0.01$.

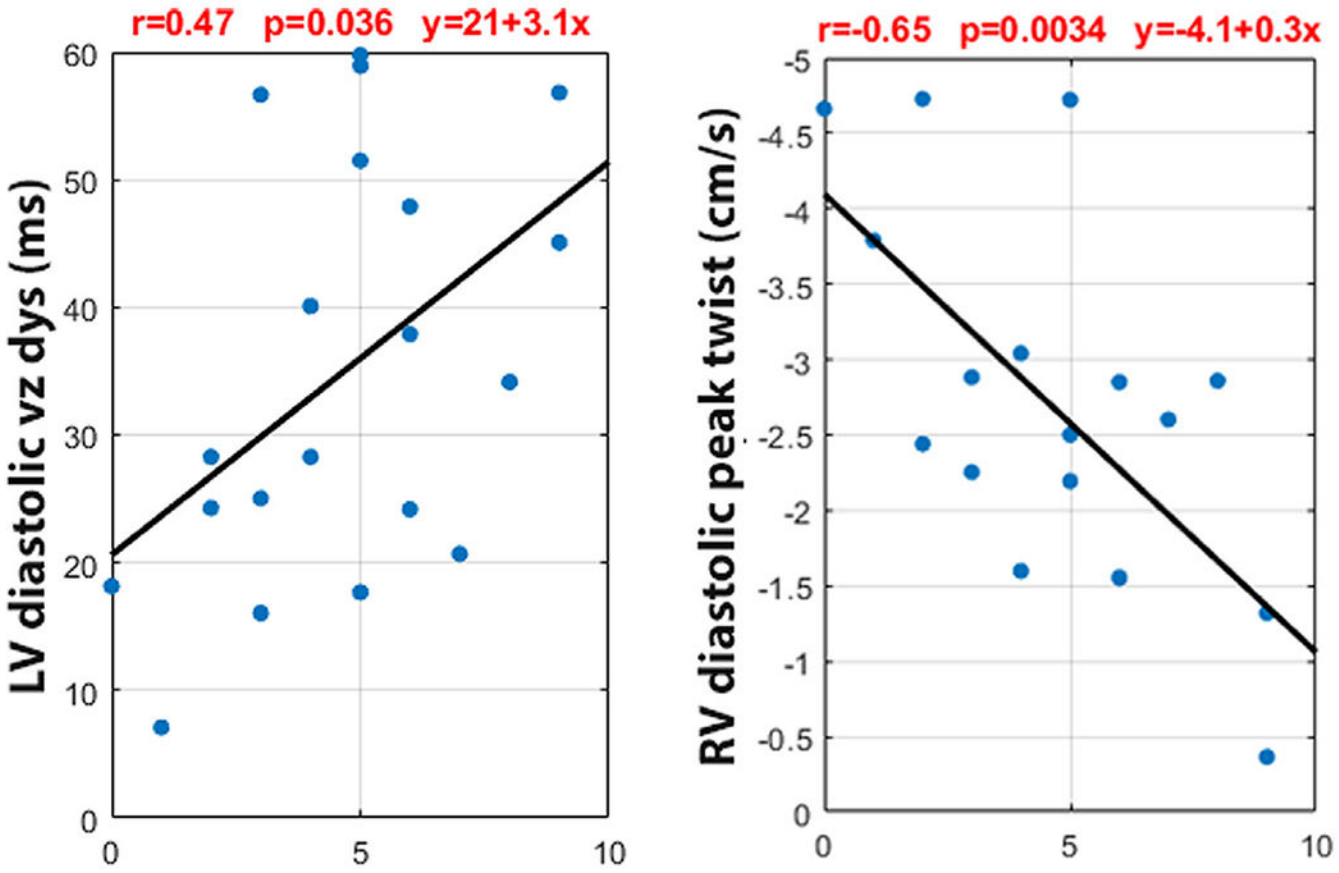

FIGURE 5:

Correlation plots showing the relationship between the LV diastolic long-axis dyssynchrony and RV diastolic peak twist to the number of rejection episodes for Htx patients. The Pearson correlation value (r) was 0.47 and −0.65, respectively, and P of 0.036 and 0.0034. LV: left ventricle, vz: long-axis, dys: dyssynchrony, RV, right ventricle.

TABLE 1.

Summary of the Demographic and Ventricular Volumetric and Function Data for Htx Patients and Controls

Demographics	**Htx patients**	**Controls**	***P*-value**
Total number (gender)	20 (11 males)	18 (9 males)	0.77
Age (years)	16.0 ± 3.1	15.5 ± 4.3	0.66
LV ESVI (mL/m2)	32.4 ± 9.6	36.8 ± 5.5	0.12
EDVI (mL/m2)	77.5 ± 13.5	86.8 ± 13.2	**0.049**
SVI (mL/m2)	45.1 ± 8.7	50.0 ± 3.2	0.11
EF (%)	58.3 ± 7.1	57.5 ± 3.2	0.65
RV ESVI (mL/m2)	33.1 ± 9.3	37.9 ± 8.4	0.11
EDVI (mL/m2)	76.8 ± 13.6	85.4 ± 15.3	0.15
SVI (mL/m2)	43.8 ± 8.2	47.6 ± 9.1	0.23
EF (%)	57.2 ± 7.3	55.8 ± 4.6	0.52
Time after Htx	5.9 ± 5.4		
Total number of rejection episodes (ACAR History)	4.7 ± 2.4		

All values report as means ± standard deviations. LV: left ventricle; RV: right ventricle; ESVI: end-systolic indexed volume; EDVI: end-diastolic indexed volume; SVI: indexed stroke volume; EF: ejection fraction; ACAR: acute allograft rejection. Significant differences are highlighted in bold.

TABLE 2.

Comparison of Global Velocities Between Htx Patients and Controls

Global velocity comparisons			Htx patients	Controls	*P*-values
LV	Systole	vr (cm/s)	3.0 ± 0.5	3.1 ± 0.5	0.55
		vz (cm/s)	4.6 ± 1.6	6.3 ± 1.7	**0.003**
		twist (cm/s)	2.2 ± 0.7	2.5 ± 0.8	0.14
	Diastole	vr (cm/s)	−4.7 ± 0.7	−5.1 ± 0.6	0.08
		vz (cm/s)	−5.1 ± 1.3	−8.2 ± 1.4	< **0.001**
		twist (cm/s)	−3.3 ± 1.0	−3.6 ± 1.2	0.33
RV	Systole	vr (cm/s)	3.9 ± 1.1	5.4 ± 1.6	0.07
		vz (cm/s)	3.2 ± 1.1	5.4 ± 1.6	< **0.001**
		twist (cm/s)	1.9 ± 1.1	3.6 ± 1.8	**0.002**
	Diastole	vr (cm/s)	−4.4 ± 0.6	−4.8 ± 0.6	0.06
		vz (cm/s)	−2.4 ± 0.6	−5.9 ± 1.5	< **0.001**
		twist (cm/s)	−2.7 ± 1.2	−3.9 ± 1.3	**0.007**

Significant differences are highlighted in bold. Htx, heart transplant; LV, left ventricle; RV, right ventricle; vr, radial velocity; vz, long-axis velocity.

TABLE 3.

Pearson Correlations Between Global Function Parameters and TPM Global Velocities for Htx Patients

			LVEDVI	LVESVI	LVSVI	LVEF	RVEDVI	RVESVI	RVSVI	RVEF
LV	Systole	vr	0.31	0.15	**0.71**	**0.47**	0.39	−0.03	**0.65**	**0.52**
		vz	0.03	−0.01	0.26	0.25	0.09	−0.03	0.17	0.2
		twist	0.14	−0.09	**0.65**	**0.69**	0.36	0.01	**0.56**	**0.48**
	Diastole	vr	**0.48**	0.32	0.41	0.11	0.42	0.15	**0.53**	0.29
		vz	0.08	0.14	0.1	−0.09	0.09	0.06	0.1	0.08
		twist	0.17	0.14	0.33	0.18	0.24	0.17	0.23	0.17
RV	Systole	vr	0.11	0.07	0.44	0.29	0.06	−0.29	0.36	**0.58**
		vz	0.05	0.04	0.25	0.17	0.01	−0.2	0.22	0.4
		twist	0.29	0.2	**0.59**	0.42	0.38	−0.004	**0.62**	**0.53**
	Diastole	vr	−0.07	0.01	−0.11	−0.13	−0.22	−0.31	−0.07	0.28
		vz	−0.25	−0.17	−0.22	−0.05	−0.34	−0.34	−0.2	0.23
		twist	−0.16	−0.04	0.2	0.23	0.004	−0.06	0.06	0.18

Significant correlations ($P < 0.05$) are highlighted in bold.

*$P < 0.05$;

**$P < 0.01$.

LVEDVI: left ventricle end-diastolic volume indexed, LVESVI: left ventricle end-systolic volume indexed, LVSVI: left ventricle stroke volume indexed, LVEF: left ventricle ejection fraction, RVEDVI: right ventricle end-diastolic volume indexed, RVESVI: right ventricle end-systolic volume indexed, RVSVI: right ventricle stroke volume indexed, RVEF: right ventricle ejection fraction, vr: radial velocity, vz: long-axis velocity.